Memorias del 2023 Congreso Nacional de Control Automático
25-27 de Octubre, 2023. Acapulco, Guerrero, México.

Design and Optimization of a PIR Controller for Voltage Regulation in a Synchronous Boost Converter

E. Moreno-Negrete * **A. Ramírez** ** **L. Félix** *
C.-F. Méndez Barrios *

* *Faculty of Engineering, Universidad Autónoma de San Luis Potosí (UASLP), México, 78290 (e-mail: emone@ieee.org, fernando.barrios@uaslp.mx).*
** *CONAHCYT-Division of Control and Dynamical Systems, IPICYT, México, 78216 (e-mail: adrian.ramirez@ipicyt.edu.mx)*

Abstract: This paper proposes a proportional-integral-retarded (PIR) controller for a synchronous boost converter to ensure its reliable operation during voltage regulation. The PIR controller is based on the addition of a time-delay as a design parameter. In this approach, we analyze the spectral properties of the closed-loop system and establish a tuning rule that optimizes its dynamic response, thus maximizing the exponential decay rate for the system's solutions. Inspired by the application field of renewable energy systems such as *photovoltaic and fuel-cell systems*, we validate the significance of our results via numerical simulations and show that incorporating delays as design parameters improves relative stability margins.

Keywords: Delay-based control, renewable energy systems, power electronic systems

1. INTRODUCTION

Decarbonizing the power sector is of major importance for mitigating global warming in the coming decade. To achieve this, emerging technologies such as electric vehicle charging stations (LaMonaca and Ryan, 2022), renewable energy systems (Tan and Mohamad-Saleh, 2023), and fuel cell-based propulsion systems (Issi and Kaplan, 2022) are being integrated into the electrical network. However, due to intermittency in power production, these applications must incorporate step-up DC/DC converters to regulate the output voltage. In this regard, control algorithms are essential to maintain the *system's stability* while achieving specific *performance levels* during energy interruptions, as shown in Fig. 1.

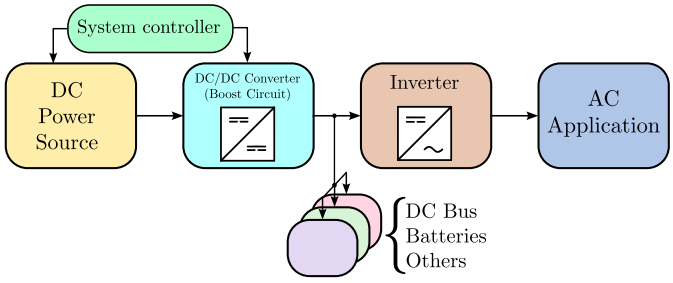

Fig. 1. Basic flow of a power supply and management scheme involving power generation, conversion, storage, management, and distribution.

Proportional-integral-derivative (PID) controllers are widely used in power electronics to maintain system's stability. These controllers provide a flexible framework for adjusting the controller gains to achieve specific objectives, such as improved stability margins and disturbance rejection capabilities, (Díaz-Rodríguez et al., 2019). Various graphical tuning techniques are available to obtain controllers that ensure stability and desirable closed-loop characteristics. One such technique is the $\mathcal{D}-$decomposition method, which has been recently applied in power electronic systems, using a PI controller to enhance gain and phase margins, reduce overshoot, and improve robustness against model uncertainties (Najdek and Nalepa, 2021). Interestingly, the derivative part of the PID controller has been disregarded in this context. The main reason for neglecting the derivative action is its sensitivity to high-frequency measurement noise, which is common in power electronic systems. As a result, the focus has been on either using PI controllers exclusively, or incorporating low-pass filters while keeping D controllers (Hägglund, 2013) to obtain reasonable control performance in noisy environments. Although controllers that include a derivative action offer desirable dynamic features, their practical implementation is often discouraged. Consequently, there is a need to search for fast closed-loop dynamic responses without relying on derivative terms.

However, it is important to note that achieving an optimal response may not be recommended in the presence of

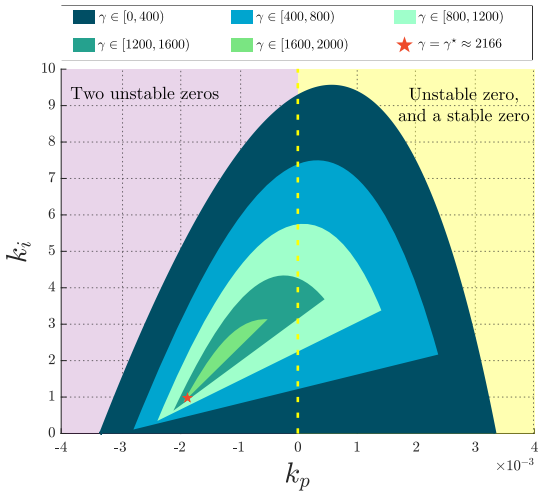

Fig. 2. $\mathcal{D}$-decomposition of the space of the space of parameters for a boost converter in closed-loop with a PI controller. The figure shows the decomposition of the $(k_p, k_i)-$space associated with the controller design parameters. The maximum exponential decay rate that the system can achieved is marked with a $\star$ symbol.

non-minimum phase zeros. Consider, for instance, a synchronous boost converter with a PI controller. In Fig. 2, the stable region in the (k_p, k_i) parameter space is represented by the blue-filled D-shaped region. Observe that searching for faster dynamic responses reduces the size of the stable region. Moreover, attempting to attain an optimal response, as indicated with a $\star$ symbol, introduces an additional unstable zero, resulting in poor converter performance. Therefore, careful consideration is necessary when choosing control strategies for systems with non-minimum phase zeros, as optimizing the response can come at the cost of stability and system performance (Moreno-Negrete et al., 2021).

On the other hand, recent studies highlight the potential of modified PID controller structures that include intentional delays to increase stability margins and achieve optimal responses without introducing undesired unstable zeros or amplifying measurement noise (Hernández-Gallardo et al., 2023; Hernández-Díez et al., 2020; Michiels et al., 2023). As suggested in (Ramirez et al., 2015), a traditional PID controller can be replaced by a proportional-integral-retarded (PIR) controller, which has shown promise in power systems as demonstrated in (Moreno-Negrete et al., 2022) and (Ramírez, 2023). These findings emphasize the potential of delay-based controllers and demonstrate their capacity not only to provide stability in power electronic systems, but also to maintain a balance between performance and robustness. This balance remains an open challenge in the field.

To address the design challenge described above, we propose employing a widely studied class of converters, specifically a synchronous boost converter in closed-loop

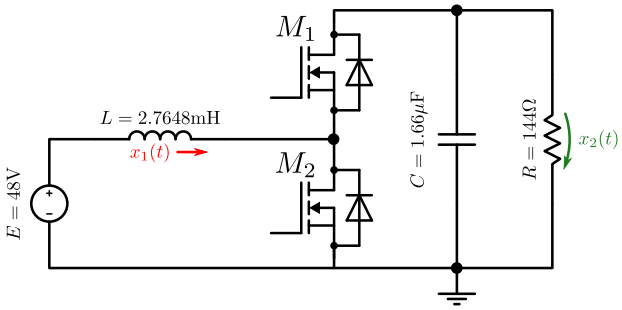

Fig. 3. Synchronous boost DC-DC converter, step-up ratio 48V-120V.

with a PIR controller. Recent studies have highlighted PIR controllers' capabilities to optimize the speed of response. However, the boost converter model presents an unstable zero, making it challenging to derive analytic formulas for the PIR controller parameters. Therefore, this paper presents a systematic approach to overcome this problem by utilizing spectral analysis (Ramírez et al., 2015; Villafuerte et al., 2012). Our focus lies in obtaining tuning formulas that can be computed with a finite number of operations. To the best of the authors' knowledge, no comparable findings in the existing literature specifically address non-minimum phase systems. By developing computationally efficient tuning formulas, our work provides a valuable solution to the PIR design problem, effectively addressing the challenges introduced by the presence of unstable zeros in the boost converter model.

The rest of the paper is organized as follows: Section 2 introduces mathematical descriptions and definitions related to the proposed controller. These provide a foundation for understanding the controller's operation. In Section 3, motivated by previous research findings, we present the γ-stability approach for tuning the PIR controller parameters. Section 4 utilizes the tuning formulas obtained in Section 3 to testify the results over various case studies. Concluding remarks are discussed in Section 5.

2. PRELIMINARIES

The synchronous boost converter depicted in Fig.3 is a variant of the conventional boost DC-DC converter that incorporates two synchronized on-off switching devices instead of diodes to improve the efficiency with low power dissipation of MOSFET's, and performance of the converter (Dobkin et al., 2014). The converter consists of a power supply source, E, switching components M_1 and M_2, passive elements L, C, and a load resistance R.

In this note, we consider the widely recognized state-space averaging technique introduced by Middlebrook and Cuk (1976) to derive an average model for the boost converter. After applying standard simplifications, we obtain the transfer function that relates the output voltage to the duty cycle as

$$G_{vd}(s) := \beta \cdot \frac{(1 - zs)\,\omega_o^2}{s^2 + \frac{\omega_o}{Q}s + \omega_o^2}, \tag{1}$$

where the DC gain $\beta > 0$, the natural frequency of the system $\omega_o > 0$, the unstable zero $1/z > 0$ and, the quality factor of the converter $Q > 0$ are defined by

$$\begin{aligned} \beta &:= \frac{E}{(1-D)^2}, \quad \omega_o := \frac{(1-D)}{\sqrt{LC}}, \\ z &:= \frac{L}{(1-D)^2 R}, \quad Q := (1-D)R\sqrt{\frac{C}{L}}. \end{aligned} \tag{2}$$

We next adopt a control strategy using a PIR controller to address the challenges with the derivative action in electronic converters. The PIR controller given by

$$U(s) := k_p\tilde{E}(s) + \frac{k_i}{s}\tilde{E}(s) - k_r e^{-hs}\tilde{E}(s), \tag{3}$$

replaces the pure derivative action in a PID controller by using an artificial delay as a design parameter. Here, $h > 0$ is the delay, $(k_p, k_i, k_r) \in \mathbb{R}^3$ are the proportional, integral, and retarded gains, respectively, and $\tilde{E}(s)$ is the error signal. Taking into account the proposed control, the closed-loop transfer function can be expressed as

$$H(s) = \frac{\left(k_p s + k_i - k_r s e^{-hs}\right) N(s)}{sD(s) + \left(k_p s + k_i - k_r s e^{-hs}\right) N(s)}, \tag{4}$$

where $N(s)$ and $D(s)$ are, respectively, the numerator and denominator of the system in (1). Hence, the closed-loop characteristic function Δ reads

$$\Delta(s, k_r, h) := P_0(s) + P_1(s)k_r e^{-sh}, \tag{5}$$

where

$$\begin{aligned} P_0(s) &:= s^3 + s^2\left(\frac{\omega_o}{Q} - \beta\omega_o^2 k_p z\right) \\ &\quad + s\left(\omega_o^2 + (k_p - k_i z)\,\beta\omega_o^2\right) + \beta k_i \omega_o, \\ P_1(s) &:= \beta\omega_o^2\left(zs^2 - s\right). \end{aligned}$$

Assumption 1. The polynomials $N(s)$ and $D(s)$ do not have roots in common.

Remark 1. Observe that if Assumption 1 is not fulfilled, this implies the existence of a polynomial factor $R(s)$ with $\deg(R(s)) \geq 1$, such that $N(s) = R(s)\widetilde{N}(s)$ and $D(s) = R(s)\widetilde{N}(s)$. Under such a situation, choosing $R(s)$ to be of the highest possible degree, the analysis can be pursued if $R(s)$ is a Hurwitz polynomial, otherwise, the system will remain unstable independently of the control action.

Considering Assumption 1, this study focuses on optimizing system performance by analyzing (5) using frequency-domain analysis. Specifically, we rely on the graphical $\mathcal{D}-$decomposition method to propose a practical tuning methodology for the parameters of the PIR controller considering unstable zeros.

Before proceeding further, we introduce the following useful definitions:

Definition 2. (Stability crossing boundaries). A collection of points (h, k_r) is a stability crossing boundary if, for any point on the boundary, there exists an $\omega \in \mathbb{R}$, such that the characteristic equation satisfies

$$\Delta(j\omega, k_r, h) = P_0(j\omega) + P_1(j\omega)k_r e^{-j\omega h} = 0. \tag{6}$$

Definition 3. (Crossing points). Let $\mathcal{S}$ be the collection of all the stability crossing boundaries, then any point $(h, k_r) \in \mathcal{S}$ is a crossing point.

Definition 4. (Frequency crossing set). The frequency crossing set $\Omega \subset \mathbb{R}$, is the set of all ω such that, there exists at least a pair $(h, k_r) \in \mathbb{R}_+ \times \mathbb{R}$ for which

$$\Delta(j\omega, kr, h) = 0.$$

The reader is referred to (Villafuerte et al., 2012; Bhattacharyya and Keel, 1995; Gu et al., 2003; Michiels and Niculescu, 2014) for additional related literature.

3. MAIN RESULTS

In order to derive our main results, let us consider the change of variable $s \to s - \gamma$ into Δ in (5). Then, the shifted characteristic equation reads

$$\hat{\Delta}(s, \gamma, k_r, h) = P_0(s, \gamma) + P_1(s, \gamma)k_r e^{-hs}e^{h\gamma} = 0. \tag{7}$$

Remark 2. For convenience, in (7), we have adopted the notations $P_0(s, \gamma) := P_0(s - \gamma)$ and $P_1(s, \gamma) := P_1(s - \gamma)$.

Note that investigating the γ-stability of Δ is equivalent to investigating the stability of $\hat{\Delta}$. Therefore, in what follows, we first search for the crossing points (h, k_r).

Proposition 5. Let (k_p, k_i) be chosen *a priori*. Then, for a fixed $\gamma > 0$ and $\omega \in \Omega \setminus \{0\}$ the corresponding crossing points are given by

$$h(\omega, \gamma) = \frac{1}{\omega}\Big(\angle P_1(j\omega, \gamma) - \angle P_0(j\omega, \gamma) + \frac{\pi}{2}(4m + \lambda + 1)\Big), \tag{8}$$

$$k_r(\omega, \gamma) = \lambda e^{-\gamma h}\left|\frac{P_0(j\omega, \gamma)}{P_1(j\omega, \gamma)}\right|, \tag{9}$$

where, $m = 0, \pm 1, \pm 2, \ldots$, and $\lambda = \pm 1$. Furthermore, for any $h > 0$, the exponentially decaying curve

$$k_r(0, \gamma) = -e^{-\gamma h}\frac{P_0(0, \gamma)}{P_1(0, \gamma)}. \tag{10}$$

is also a crossing point.

Proof. Let γ and ω be fixed values. Then, (8) and (9) are obtained using the module and argument on both sides of (7). Finally, (10) follows from (7) by setting $s = 0$. □

3.1 Explanatory example

The relationship between $k_r(\omega, \gamma)$, $h(\omega, \gamma)$, and $k_r(0, \gamma)$ can be visually analyzed in the (h, k_r) plane, which depends on the frequencies ω and the decay rate γ. Fig. 4 shows three scenarios with graphical representations. In the first scenario, a fixed pair of gains is used: $k_p = 0.001$ and $k_i = 2.93$. By examining the graph, we can observe how different frequency sets impact the values of k_r and

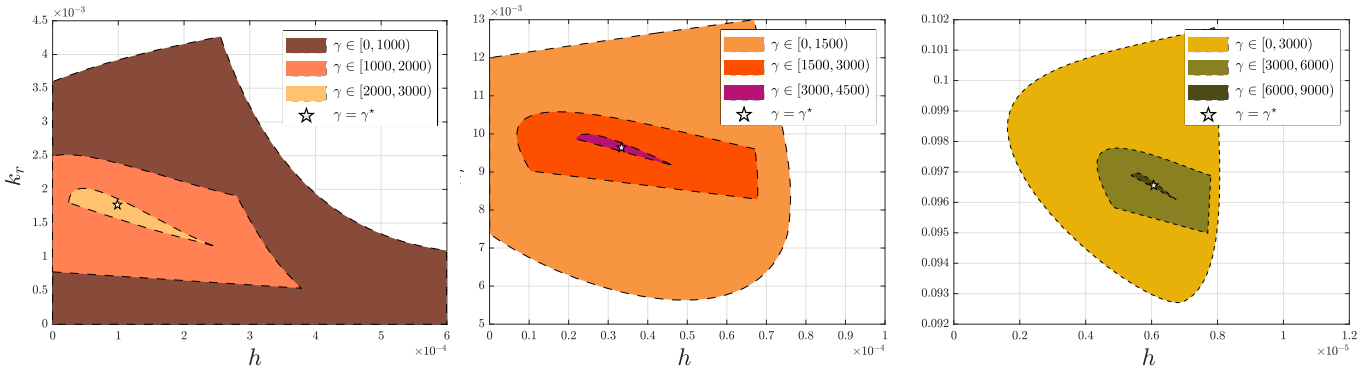

(a) (b) (c)

Fig. 4. Stability regions associated with the boost converter in closed-loop with a PIR controller for different gain values. (a) $k_p = 0.001, k_i = 2.93$. Maximum decay rate $\gamma^\star = 3970.72$. (b) $k_p = 0.01, k_i = 5$. Maximum decay rate $\gamma^\star = 4950.76$. (c)$k_p = 0.1, k_i = 15$. Maximum decay rate $\gamma^\star = 9397.63$.

h. In the second scenario, the gains are increased to $k_p = 0.01$ and $k_i = 5$, while the third case further increments the gains to $k_p = 0.1$ and $k_i = 15$. Analyzing these cases provides insights into how adjusting these parameters influences the system's behavior. As the decay rate γ increases, the regions of γ-stability in the $(h, k_r)-$space gradually shrink and eventually collapse into a single point. Fig. 4 shows these collapse points with a $\star$ symbol, which corresponds to the maximum exponential decay rate, $\gamma^\star$, that the system can achieve. In addition, this point is characterized by a triple real root assignment (Oaxaca-Adams and Villafuerte-Segura, 2023; Villafuerte et al., 2012; Ramirez et al., 2015).

Proposition 6. If $\gamma^\star$ exists, the stability domain collapses for $\gamma^\star$ such that

$$\gamma^\star \in \{\gamma_i > 0 : \mathcal{A}(\gamma_i) = 0\} \tag{11}$$

where

$$\begin{aligned}\mathcal{A}(\gamma) := a_8\gamma^8 + a_7\gamma^7 + a_6\gamma^6 + a_5\gamma^5 \\ + a_4\gamma^4 + a_3\gamma^3 + a_2\gamma^2 + a_1\gamma + a_0,\end{aligned} \tag{12}$$

with coefficients a_i, $i = 0, \ldots, 8$, given in Appendix A.

Proof. The existence of three roots at $-\gamma^\star$ implies that $\hat{\Delta} = \partial\hat{\Delta}/\partial s = \partial^2\hat{\Delta}/\partial s^2 = 0$ at $s = 0$. From these conditions we obtain that

$$k_r e^{\gamma h} = -\frac{P_0(s,\gamma)}{P_1(s,\gamma)}\bigg|_{s=0}, \tag{13}$$

$$hk_r e^{\gamma h} = -\frac{\partial}{\partial s}\left(\frac{P_0(s,\gamma)}{P_1(s,\gamma)}\right)\bigg|_{s=0}, \tag{14}$$

$$h^2 k_r e^{\gamma h} = -\frac{\partial^2}{\partial s^2}\left(\frac{P_0(s,\gamma)}{P_1(s,\gamma)}\right)\bigg|_{s=0}. \tag{15}$$

After some algebraic manipulations, one can eliminate the explicit dependence of (13)-(15) on h and k_r to finally obtain the polynomial $\mathcal{A}(\gamma)$ in (12), the roots of which qualifies as the maximum exponential decay rate. □

Corollary 7. The maximum exponential decay rate of the closed-loop system is achieved in the $(h, k_r)-$plane with

$$\begin{aligned} h &= \frac{-b_4{\gamma^\star}^4 - b_3{\gamma^\star}^3 + b_2{\gamma^\star}^2 - b_1\gamma^\star - b_0}{-c_4{\gamma^\star}^5 + c_3{\gamma^\star}^4 + c_2{\gamma^\star}^3 + c_1{\gamma^\star}^2 + c_0\gamma^\star}, \\ k_r &= -\frac{-{\gamma^\star}^3 + d_2{\gamma^\star}^2 - d_1\gamma^\star + d_0}{e^{\gamma^\star h^\star}\left(\beta{\gamma^\star}^2 z\omega_o^2 + \beta\gamma^\star\omega_o^2\right)}, \end{aligned} \tag{16}$$

where $\gamma^\star$ is obtained from (11) and the coefficients b_i, $i = \overline{0,4}$, c_i, $i = \overline{0,4}$, d_i, $i = \overline{0,2}$, are given in Appendix A.

Proof. By obtaining the solutions of the polynomial $\mathcal{A}(\gamma)$ and using the stability boundaries associated with the characteristic function $\hat{\Delta}$, we select a suitable solution for $\gamma^\star$. Then, both equations in (16) follow straightforwardly from (13)-(14). □

4. NUMERICAL EXAMPLES

To illustrate the effectiveness of the proposed results, we present several numerical examples considering the electrical specifications for the proposed converter summarized in Table 1. Numerical simulations are conducted using PLECS/PLEXIM as shown in Fig. 5.

Remark 3. We note that the synchronous boost converter can operate bidirectionally. Nevertheless, for the purpose of this analysis, we focus exclusively on its direct operation to explore the equations and parameters associated with unidirectional DC-DC.

Table 1. Parameters of the converter.

Parameter	Symbol	Value
Switching frequency	f_s	150kHz
Voltage input	E	48V
Duty cycle	D	0.6
Power	P	100W
Inductor	L	2.7648mH
Capacitor	C	1.66μF
Resistance	R	144Ω

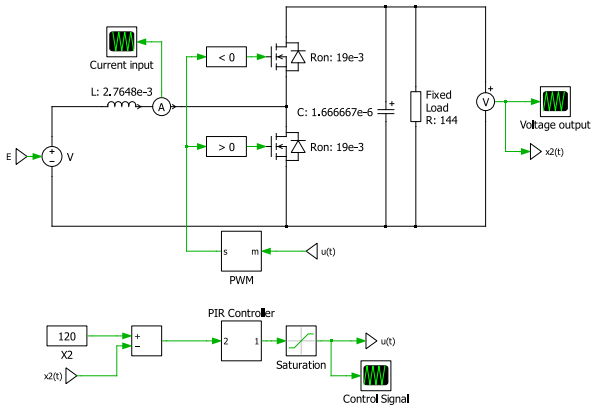

Fig. 5. System and controller benchmark simulation in PLECS.

With Remark 3 in mind, we next investigate two specific behaviors during a simulation period of 50 ms; we note that no parasitic elements in the components are considered in all cases and a saturation block of 0-1V is incorporated at the output of the controller to restrict the control signal within the predefined range. Firstly, the convergence of the system's state towards its reference is observed when the converter initiates with the controller set to zero initial conditions for all three proposed controller configurations and a PI controller tuned with $k_p = 0.001, k_i = 2.93$ which is selected to avoid introducing additional unstable zeros. Secondly, considering the desired output voltage $X_2 = E/(1-D) = 120$V, we make step increments in X_2 from its nominal value by varying E every 10 ms, reaching 100V, 40V, 70V, and subsequently settling at 48V after 40 ms, as depicted in Fig. 6. These step changes aim to emulate the dynamic response of the system to potential fluctuations commonly encountered in renewable energy sources such as solar panels or fuel-cell stacks (Ramirez, 2022).

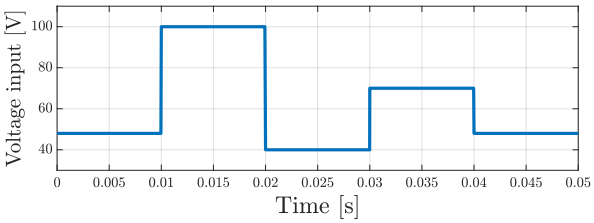

Fig. 6. Voltage-output response comparison with a PI and PIR controllers.

Then, in Fig. 7, we show how the system performs in different scenarios. In the first experiment, we compare the performance of the system subject to a PI controller with the same k_p and k_i values used in the PIR controller. We observe slower settling times and oscillations in the output response. We also obtain faster convergence times to the reference during the startup phase and reduced overshoots and undershoots in cases 2 and 3. In Case 3,

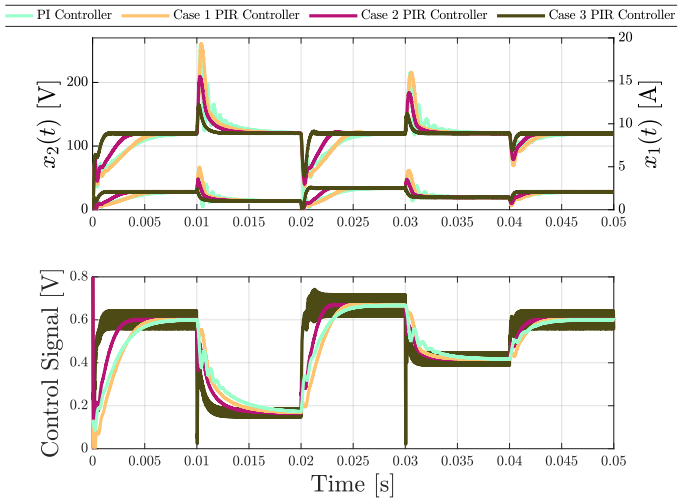

Fig. 7. Comparative evolution of voltage output $x_2(t)$, inductor current $x_1(t)$, and control signal over time with a PI and PIR controllers.

with gains $k_p = 0.1$ and $k_i = 15$, we note a faster response compared to the first two cases. It is worthy of mention that the control signal remains within a bounded region. We conclude this section by noting that our study does not account for high-frequency transitions, and therefore, we have not considered a minimum switching frequency.

5. CONCLUSIONS

We present a method to ensure the exponential stability of a PIR controller when controlling a synchronous boost converter model with unstable zeros. Through spectral methods, we conduct a stability analysis and derive an analytical tuning formula for the PIR controller parameters based on the maximum exponential decay rate that the closed-loop system can achieve. Numerical results demonstrate that the PIR controller improves stability margins without introducing noise amplification issues. Future research directions include the experimental verification of the findings and further formalization of the developments.

The present analysis revolves around a regulation problem in DC-DC converters. However, in the context of DC-AC and AC-DC converters, additional challenges arise due to direct and alternating current conversion. One of these challenges requires solving a tracking problem and one possibility to address this problem involves a change of coordinates using well-known *DQ transformations*. In the DQ-coordinate frame, tracking problems can be understood as regulation problems, rendering our results applicable in this case.

Appendix A. COEFFICIENTS

In this section, we provide the following list of equations used in *Proposition 6* and *Corollary 7*

$$
\begin{aligned}
a_0 &:= Q^2\beta^2k_i^2\omega_o^4,\\
a_1 &:= 4\beta\omega_o^4k_i\left(\beta k_iz-\frac{1}{2}\beta k_p-\frac{1}{2}\right)Q^2,\\
a_2 &:= 6\beta\omega_o^3k_iQ\left(\frac{2}{3}+z\omega_o\left(\beta k_iz-\frac{4}{3}\beta k_p-\frac{2}{3}\right)Q\right),\\
a_3 &:= 4\left(\left(-2+z^2\left(\beta k_iz-3\beta k_p-1\right)\omega_o^2\right)Q+2z\omega_o\right)\beta\omega_o^2k_iQ,\\
a_4 &:= \omega_o^2\left(-1+\left(2+\left(1+z^2k_i^2\beta^2+2k_i\left(-4\beta^2k_p-\beta\right)z\right.\right.\right.\\
&\quad \left.\left.\left.+2\beta k_p\right)z^2\omega_o^2-18\beta k_iz+2\beta k_p\right)Q^2\right.\\
&\quad \left.+6\left(k_iz+\frac{k_p}{3}\right)\beta\omega_ozQ\right),\\
a_5 &:= 2\left(\left(z^2k_p\beta\left(\beta k_iz-1\right)\omega_o^2+7\beta k_iz-\beta k_p-2\right)z\omega_oQ^2\right.\\
&\quad \left.+\left(-1-z^2\left(\beta k_iz+\beta k_p-1\right)\omega_o^2\right)Q+z\omega_o\right)\omega_o,\\
a_6 &:= 2\left(\left(1+2\left(\beta k_iz^3-z^2\right)\omega_o^2\right)Q^2-2z\omega_oQ\right),\\
a_7 &:= 4Q^2z, a_8=Q^2z^2.
\end{aligned}
\tag{A.1}
$$

$$
\begin{aligned}
b_0 &:= \beta k_i\omega_o^2Q,\ b_1=2Q\beta k_iz\omega^2,\\
b_2 &:= \left(-z\omega_o^2(\beta k_iz-1)Q+\omega_o\right),\ b_3=2Q,\ b_4=Qz.\\
c_0 &:= \beta k_i\omega_o^2,\ c_1=Q\beta k_iz\omega_o^2+Q\omega_o^2\left(-1+\left(k_iz-k_p\right)\beta\right),\\
c_2 &:= Q\omega_o^2\left(-1+\left(k_iz-k_p\right)\beta\right)z-Q\beta k_pz\omega_o^2+\omega_o,\\
c_3 &:= -Q\beta k_pz\omega_o^2+\omega_oz-Q,\ c_4=Qz,\\
d_2 &= \frac{\omega_o}{Q}-\beta k_pz\omega_o^2,\\
d_1 &:= \left(-\beta k_iz\omega_o^2+\beta k_p\omega_o^2+\omega_o^2\right),\\
d_0 &:= \beta k_i\omega_o^2.
\end{aligned}
\tag{A.2}
$$

REFERENCES

Bhattacharyya, S.P. and Keel, L.H. (1995). Robust control: the parametric approach. In *Advances in control education 1994*, 49–52.

Díaz-Rodríguez, I.D., Han, S., and Bhattacharyya, S.P. (2019). *Analytical design of PID controllers*. Springer.

Dobkin, B., Hamburger, J., et al. (2014). Analog circuit design volume three. Technical report, Elsevier Science.

Gu, K., Chen, J., and Kharitonov, V.L. (2003). *Stability of time-delay systems*. Springer.

Hägglund, T. (2013). A unified discussion on signal filtering in PID control. *Control engineering practice*, 21(8), 994–1006.

Hernández-Díez, J.E., Méndez-Barrios, C.F., Niculescu, S.I., and Bárcenas-Bárcenas, E. (2020). A current sensorless delay–based control scheme for MPPT–boost converters in photovoltaic systems. *IEEE Access*, 8, 174449–174462.

Hernández-Gallardo, J.A., Guel-Cortez, A.J., Gonzalez-Galvan, E.J., and Méndez-Barrios, C.F. (2023). Designing proportional delayed integral control for fast regulation in second-order systems: A geometric approach. In *2023 9th International Conference on Control, Decision and Information Technologies*.

Issi, F. and Kaplan, O. (2022). Simulation of a wireless charging multiple e-scooters using PV array with class-e inverter fed by PI controlled boost converter for constant output voltage. In *2022 10th International Conference on Smart Grid*, 61–65.

LaMonaca, S. and Ryan, L. (2022). The state of play in electric vehicle charging services–a review of infrastructure provision, players, and policies. *Renewable and sustainable energy reviews*, 154, 111733.

Michiels, W. and Niculescu, S.I. (2014). *Stability, control, and computation for time-delay systems: an eigenvalue-based approach*. SIAM.

Michiels, W., Niculescu, S.I., and Boussaada, I. (2023). A complete characterization of minima of the spectral abscissa and rightmost roots of second-order systems with input delay. *IMA Journal of Mathematical Control and Information*.

Middlebrook, R.D. and Cuk, S. (1976). A general unified approach to modelling switching-converter power stages. In *1976 IEEE power electronics specialists conference*, 18–34.

Moreno-Negrete, E., Hernández-Díez, J., Méndez-Barrios, C., Langarica-Córdoba, D., Miranda-Vidales, H., and Félix, L. (2021). PI control scheme design of high gain transformerless DC-DC converter. In *2021 23rd European Conference on Power Electronics and Applications*.

Moreno-Negrete, E., Méndez-Barrios, C.F., Félix, L., and Ramírez, A. (2022). Some remarks on the design of robust PIR controllers for step-down DC-DC converters. *IFAC-PapersOnLine*, 55(36), 13–18.

Najdek, K. and Nalepa, R. (2021). The frequency-and the time-domain design of a dual active bridge converter output voltage regulator based on the D-decomposition technique. *IEEE Access*, 9, 71388–71405.

Oaxaca-Adams, G. and Villafuerte-Segura, R. (2023). On controllers performance for a class of time-delay systems: Maximum decay rate. *Automatica*, 147, 110669.

Ramirez, A. (2022). A robust energy processing method for fuel cell systems supplying a time-varying uncertain load. *International Journal of Energy Research*, 46(14), 19961–19979.

Ramírez, A., Garrido, R., and Mondié, S. (2015). Velocity control of servo systems using an integral retarded algorithm. *ISA transactions*, 58, 357–366.

Ramirez, A., Mondié, S., Garrido, R., and Sipahi, R. (2015). Design of proportional-integral-retarded (PIR) controllers for second-order LTI systems. *IEEE Transactions on Automatic Control*, 61(6), 1688–1693.

Ramírez, A. (2023). Performance and robustness trade-offs in PIR control of uncertain second-order systems with input disturbances. *International Journal of Control*, 0(0), 1–12. doi:10.1080/00207179.2023.2214637.

Tan, W.H. and Mohamad-Saleh, J. (2023). Critical review on interrelationship of electro-devices in PV solar systems with their evolution and future prospects for mppt applications. *Energies*, 16(2), 850.

Villafuerte, R., Mondié, S., and Garrido, R. (2012). Tuning of proportional retarded controllers: theory and experiments. *IEEE Transactions on Control Systems Technology*, 21(3), 983–990.